Industrial Crops & Products 178 (2022) 114648

Contents lists available at ScienceDirect

Industrial Crops & Products

journal homepage: www.elsevier.com/locate/indcrop

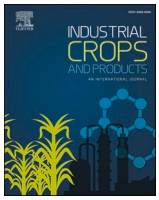

Boosting Portland cement-free composite performance via alkali-activation and reinforcement with pre-treated functionalised wheat straw

Mehdi Chougan [a], Seyed Hamidreza Ghaffar [a,*], Pawel Sikora [b,c], Ewa Mijowska [d], Wojciech Kukułka [d], Dietmar Stephan [b]

[a] Department of Civil and Environmental Engineering, Brunel University London, Uxbridge UB8 3PH, United Kingdom
[b] Building Materials and Construction Chemistry, Technische Universität Berlin, Gustav-Meyer-Allee 25, 13355 Berlin, Germany
[c] Faculty of Civil and Environmental Engineering, West Pomeranian University of Technology in Szczecin, Al. Piastow 50, 70-311 Szczecin, Poland
[d] Department of Nanomaterials Physicochemistry, Faculty of Chemical Technology and Engineering, West Pomeranian University of Technology, Al. Piastow 45, 70-311 Szczecin, Poland

ARTICLE INFO

Keywords:
Alkali-activated materials
Wheat straw
Attapulgite nanoclay
Graphene nanoplatelets
Pre-treatment
Surface functionalisation

ABSTRACT

Utilising wheat straw reinforced OPC-free composites in the construction industry requires efficient, eco-friendly pre-treatment coupled with surface functionalisation methods to turn it into a high-performance material. Herein, alkali-activated material (AAM) was used as an OPC-free matrix, while eco-friendly hybrid pre-treatment and surface functionalisations were applied to mitigate the surface quality deficiencies of wheat straw and improve its compatibility with low-carbon binders. Wheat straw particles were subjected to a mild physical pre-treatment (hot-water followed by steam) and surface functionalisation using attapulgite nanoclay and graphene nanoplatelets to improve their capacity as an effective reinforcing material in AAM. Comprehensive characterisation verified successful pre-treatment and surface functionalisation, which led to the improved interfacial bond between wheat straw and AAM. The best results were obtained for the AAM samples reinforced with pre-treated straw that was functionalised with attapulgite nanoclay (i.e., H+S-AT), in which the volume of permeable voids decreased by 18%, while compressive and flexural strength at 90 d increased by 41% and 27%, respectively, compared to the control sample. However, the effect on the thermal properties of the resulted composites was not significant.

1. Introduction

With the growing population and the increasing space requirements per person, the construction material business has seen a remarkable increase in demand, particularly in the previous decade. However, sufficient attention has not been paid to adopting low-carbon building materials (Albar et al., 2020; Chougan et al., 2021, 2020b; Sikora et al., 2021). The production of traditional building materials (e.g., bricks, cement (OPC), and steel rebars) demands large quantities of thermal and electrical energy, polluting the land, air, and water. Life Cycle Assessment (LCA) studies have shown that alkali-activated materials (AAMs) include considerable potential for minimizing the climate change implications of the cement manufacturing process. The results revealed that AAMs produce a substantially lower carbon footprint than OPC-based combinations leading to an approximately 93% reduction in global warming potential. AAM utilisation also reduces terrestrial ecotoxicity potential, abiotic depletion potential element, and abiotic depletion potential fossil by 77%, 34%, and 49%, respectively (McLellan et al., 2011; Meshram and Kumar, 2021; Ouellet-Plamondon and Habert, 2015). Alkali-activated materials have recently emerged as a viable alternative to OPC-based composites in which as an aluminosilicate source binder, industrial primary products and by-products such as silica fume (SF), ground granulated blast-furnace slag (GGBS), metakaolin, and fly ash (FA) have been employed. The use of AAM with outstanding durability and mechanical performance makes them a reliable candidate for the future construction industry (da Silva Alves et al., 2019).

Recently, several types of biomass reinforcing additives collected from various sources, e.g., agricultural waste or dedicated crops, have been utilised in cementitious composite to improve their properties (Alengaram et al., 2013; Pacheco-Torgal and Jalali, 2011; Walbrück et al., 2021, 2020). Biomass materials contain chemical components such as lignin, cellulose, inorganic substances, hemicellulose, and

* Corresponding author.
E-mail address: seyed.ghaffar@brunel.ac.uk (S.H. Ghaffar).

https://doi.org/10.1016/j.indcrop.2022.114648
Received 14 October 2021; Received in revised form 31 January 2022; Accepted 2 February 2022
Available online 9 February 2022

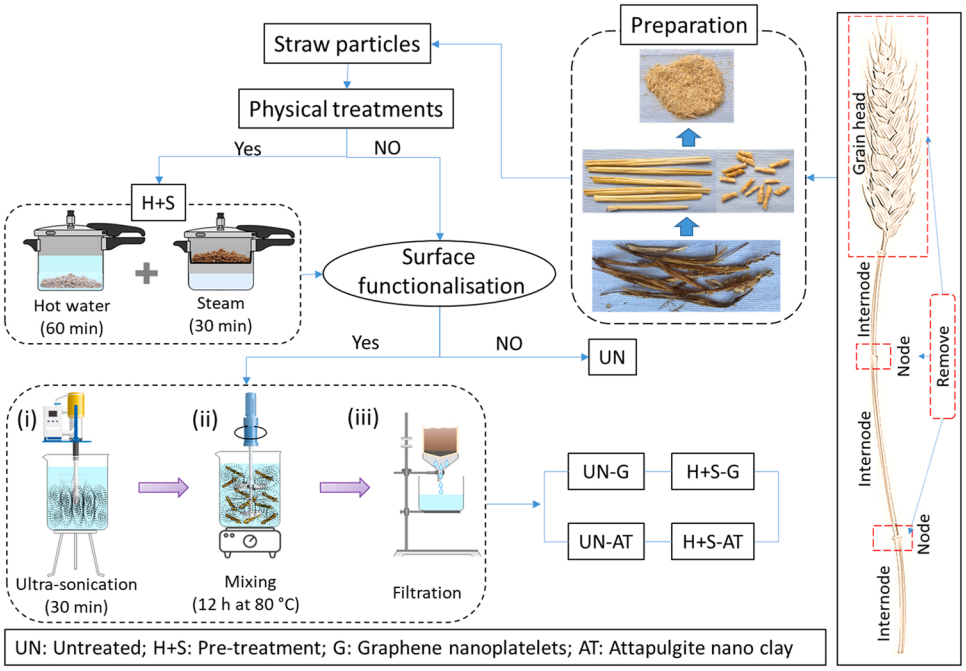

Fig. 1. Schematic framework of different stages of straw preparation.

extractives (e.g., waxes and pectins) that can affect their mechanical and physical properties (Chougan et al., 2020a; Elbashiry et al., 2018). Chemical components that cover the surface of the biomass, such as lignin, hemicellulose, and pectin, have a negative impact on the mechanical performance of the final cementitious composite. Due to the high concentration of the hydrophobic components, less pure cellulose is present, lowering the compatibility of these materials used as reinforcing agents in AAMs. As a result, biomass-AAM interfacial bonding and mechanical performance are diminished (Tian et al., 2018).

Several biomass materials including, flax shive (Khazma et al., 2014), sisal fibres (Mishra et al., 2004), hemp particles (Hakamy et al., 2016), jute fibres (Ghaffar et al., 2020; Zhou et al., 2013), bamboo fibres (Kathiravan et al., 2021), pineapple leaf fibres (Abirami et al., 2020), granular cork (Merabti et al., 2021), have been reported as promising eco-friendly reinforcing agents in cement-based composites. Recent studies have proven that the inclusion of reinforcing biomass materials in cementitious composites leads to an enhanced mechanical performance and bonding properties (Mohamed et al., 2010; Vo and Navard, 2016), and most effectively, it improves composite's physical properties, including, energy-saving (Tran Le et al., 2010), thermal insulation (Parcesepe et al., 2021), and acoustic absorption (Glé et al., 2021). Uncertainty over the long-term behaviour of biomass materials in the highly alkaline environment is one of the main challenges and limitations of utilising such materials in cementitious composites. Several other factors, such as increased temperature induced by the hydration process, formation of hydration products, mineralisation by cement suspension free cations (e.g., Ca^{2+}), degrade the lignocellulosic material's principle constituents (i.e., lignin, hemicellulose, extractives, and cellulose) lead to weakening the biomass microstructure over time (Pacheco-Torgal and Jalali, 2011). Numerous studies have proposed employing pre-treatment and coating procedures as a possible solution to overcome these drawbacks (Ghaffar et al., 2017b; Ghaffar and Fan, 2015; Hýsková et al., 2020). Many different pre-treatment techniques have been proposed to improve matrix-biomass adhesion and, therefore, the final performance of the cement-free composites, which can be broken down into physical and chemical methods. It must be noted that despite chemical pre-treatments successfully altering biomass structure when considering scalability, it might not be economically feasible, and since the required chemicals can be a pollutant, the environmental impacts would be negative. Therefore, physical pre-treatments are favourable (Chougan et al., 2020a; Fan et al., 2018). In addition, for bio-composites with polymeric matrix, using coupling agents (compatibilisers), including maleic anhydride (MA), silane, polydopamine (PDA), have also proved to be beneficial in modifying the cellulosic biomass surface (Ghaffar et al., 2018). Coupling agent materials (CA) create a chemical bond and promote interfacial bonding in composites by acting as a link between the biomass and the polymer matrix. The hydroxyl groups of CAs are able to react with the biomass's surface on one end. The other CAs functional group on the other end of CAs also bond with the polymer matrix, which leads to enhancing mechanical performance of composites' (Ghaffar et al., 2018).

Wheat straw is known as one of the most available crops by-product used as a nutrients-source for animal food and soil fertilisers. However, a considerable quantity of wheat straw is incinerated through in-situ burning each year, releasing hazardous substances such as carbon dioxide, polycyclic aromatic hydrocarbons, nitrogen oxides, and sulfur dioxide in soil and the atmosphere (Guan et al., 2020). In the UK, the area of wheat in England in 2019 was around 1.69 million hectares (i.e. harvesting 16.3 million tons of wheat), which is 4.5% increase when compared to 2018, leaving 5.5 million tons of waste annually, assuming a residue/crop ratio of 1:3 (Department for Environment Food and Rural Affairs DEFRA, 2020).

This research has two unique selling points, one is that it uses low-carbon cementitious composites and two is the use of agricultural waste to strengthen the mechanical properties of cementitious materials. The carbon emission in the construction industry is well known issue. Cement manufacturing generates a lot of greenhouse gas (GHG) emissions and wastes excessive energy. The entire manufacturing process consumes around 3.2 GJ energy/tonne. In addition, each tonne of cement generates about 810 kg of carbon dioxide (CO_2), 1.0 kg of sulphur dioxide (SO_2), and 2.0 kg of nitrogen oxides (NO_x) throughout the manufacturing process (Habert et al., 2011; Heede and Belie, 2012). Utilisation of AAM can significantly mitigate these negative effects. Moreover, AAMs with superior mechanical performance could be employed to immobilise toxic and radioactive compounds, manage waste materials, improve fire resistance, and repair structures. The ability of these materials to act as coatings for marine structures has also been confirmed. In addition, agricultural biomass particles provide a

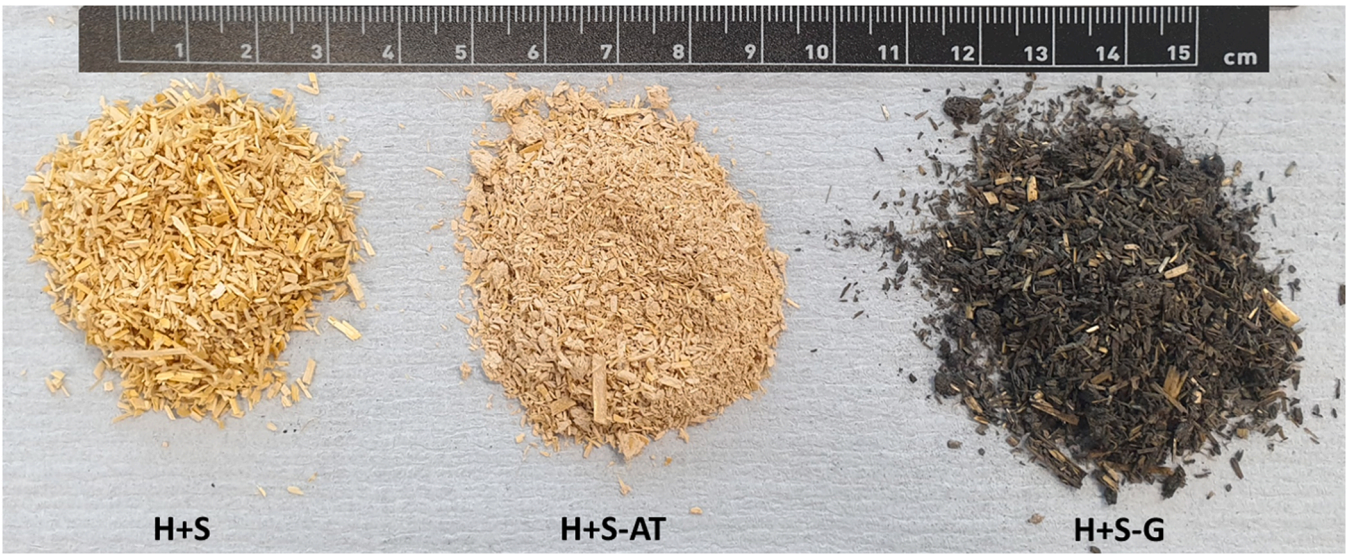

Fig. 2. Visual appearance of straw particles after pre-treatment (H+S) and subsequent surface functionalisation with attapulgite nanoclay (AT) and graphene nanoplatelets (G).

number of key benefits, including bio-renewability and biodegradability, availability at a low cost, recycling ability, non-hazardous and toxic nature, promising physical and mechanical properties, and zero carbon footprint comparing conventional reinforcement alternatives (Satyanarayana et al., 2009; Wambua et al., 2003). Due to the aforementioned remarkable features, combination of AAMs with biomass reinforcing agents have triggered a surge of interest in its prospective applications.

In this study, selective separation of wheat straw defects, i.e., nodes (see Fig. 1), was employed to improve matrix-straw bonding. The internodes were then subjected to a mild physical pre-treatment (H+S) and the surface of both pre-treated and untreated straw particles were functionalised using graphene nanoparticles and attapulgite nanoclay with the dosages of 0.1 wt.-% and 1 wt.-%, respectively. Wheat straw particles were then added to the alkali-activated materials to be tested and comprehensively characterised. To the best of the authors' knowledge, no studies on wheat straw have carried out the pre-treatment coupled with surface functionalisation using nanoparticles to be used in AAM. Wheat straw particles were characterised to evaluate and verify surface functionalisation using SEM, Raman, XRD, and TGA. In addition, bulk property tests were conducted to investigate the impact of wheat straw as a reinforcing additive on the mechanical performance, porosity, thermal properties, and microstructure of AAMs' in the hardened state.

2. Materials and methodology

Fly ash (FA) from Cemex, UK, ground granulated blast furnace slag (GGBS) from Hanson Heidelberg Cement, UK, micro-silica fume (SF) from J. Stoddard & Sons Ltd, graded sand (0 – 0.5 mm and 0.5 – 1.0 mm), sodium silicate solution with the SiO_2/Na_2O mass ratio of 3.23 (8.60 wt% Na_2O, 27.79 wt% SiO_2, 63.19 wt% H_2O, and 0.4 wt% Al_2O_3), and 10 mol/l sodium hydroxide solution were used as the ingredients of alkali-activated materials (AAM). More details on materials characterizations, including the material size distribution and compositions, can be found in the author's previous research (Albar et al., 2020; Chougan et al., 2020b). Wheat straw biomass (Triticum aestivum L.), harvested in late summer of 2019, was purchased from Middlesex, UK farms. Before the pre-treatment and surface functionalisation stages, as-received wheat straw was cleaned and oven-dried at 100 ± 5 °C for 24 h. As reported in author's previous study, for an optimised feedstock to be used in bio-based composites, only the internodes of straw stems are suitable and the nodes have to be separated, due to their morphology and surface chemical functional groups that act as defects in the context of bio-based composites (Chougan et al., 2020a; Ghaffar et al., 2017a; Ghaffar and Fan, 2015, 2013). Graphene nanoplatelets, referred here as G, supplied by Nanesa S.r.l., Italy, and attapulgite nanoclay (AT) provided by Lawrence Industries Ltd., UK, were used as coupling agents for surface functionalisations. Extensive information on the characteristics of coupling agents can be found in the author's previous studies (Chougan et al., 2021; Lamastra et al., 2021). Both G and AT materials are supposed to act as coupling agents, improving the interfacial bonding between the straw and the AAM. However, some of these components are dislodged from the straw surface during the mixing process and serve as reinforcing additives.

2.1. Wheat straw pre-treatments and surface functionalisations

2.1.1. Wheat straw pre-treatments

As shown in Fig. 1, upon cleaning and separation of internodes from the stem, both untreated and pre-treated straw stems were shredded to obtain particles with the size range between 2 mm and 5 mm using Retsch SM 100 cutting mill. Hot-water and steam (H+S) pre-treatment was used on wheat straw to investigate the effects of surface functionalisations in more detail and assess the role of pre-treatment and surface functionalisations on performance of AAM reinforced straw composites. Wheat straw particles were first boiled in hot water (H) using a pressure cooker for 60 min at a constant pressure of about 0.1 MPa. Immediately after, boiled-straw samples were removed and steamed (S) for 30 min by placing them in a mesh basket directly above boiling water.

2.1.2. Wheat straw surface functionalisation with graphene nanoplatelets and attapulgite

Prior to the surface functionalisations, graphene nanoplatelets (G) and attapulgite nanoclay (AT) were sonicated, respectively, in an aqueous solution for 90 min to ensure adequate dispersion. Untreated (UN) and pre-treated (H+S) straw samples were immersed in a pre-dispersed G and AT aqueous solution in a beaker, correspondingly (see Fig. 1-i). The concentrations of AT and G were 1 wt% and 0.1 wt%, respectively, selected based on the previous studies conducted by Scafarro et al. (2020) and Zhu et al. (2019) for G and AT, respectively (Scaffaro et al., 2020; Zhu et al., 2019). After being heated at 80 °C for 12 h under mechanical stirring (Fig. 1-ii), the mixture was filtered once and oven-dried at 80 °C for 24 h to remove the water (Fig. 1-iii). The AT and G particles were covered on the straw particles' surface during the

Table 1
Mix formulations of AAM reinforced with untreated (UN) and pre-treated (H+S) straw particles.

Name	Binder (wt.-%)			Additive (wt.-%) (of AAM)		Functionalising agents (wt.-%) (of AAM)		Aggregate (wt.-%)		Na_2SiO_3: NaOH ratio
	FA	GGBS	SF	UN straw	H+S straw	AT	G	0–0.5 mm	0.5–1 mm	
CS	60	25	15	0	0	0	0	60	40	2:1
UN	60	25	15	1	0	0	0	60	40	2:1
UN-2	60	25	15	2	0	0	0	60	40	2:1
UN-3	60	25	15	3	0	0	0	60	40	2:1
H+S	60	25	15	0	1	0	0	60	40	2:1
H+S-2	60	25	15	0	2	0	0	60	40	2:1
H+S-3	60	25	15	0	3	0	0	60	40	2:1
UN-AT	60	25	15	1	0	1	0	60	40	2:1
H+S-AT	60	25	15	0	1	1	0	60	40	2:1
UN-G	60	25	15	1	0	0	0.1	60	40	2:1
H+S-G	60	25	15	0	1	0	0.1	60	40	2:1

drying process. Fig. 2 shows the visual appearance of straw particles after surface functionalisation processes.

2.2. Alkali-activated material preparation and mixing design

Seven AAMs reinforced with wheat straw particles were produced (see Table 1). In order to make AAM composites, all binder ingredients, including FA, GGBS, and SF with a percentage of 60, 25, and 15 wt.-% respectively (of the total weight of the binder), and graded sand aggregates with two particle size distribution of 0–0.5 mm and 0.5–1 with a constant percentage of 60, and 40 wt.-%, respectively (of the total weight of the aggregates), were dry-mixed for 5 min at 350 rpm using planetary mixer. After dry mixing the wheat straw particles (1, 2, and 3 wt.-% of the weight of the binder) were added in and mixed for 5 min at 250 rpm. The alkaline solution comprised of a mixture of sodium hydroxide and sodium silicate solutions (weight ratio of 2:1) with a dosage of 40 wt.-% (of the total weight of the binder) was used as activator. The alkaline solution was gradually added to the dry mixture and stirred at 450 until a homogeneous AAM composite was obtained. It should be mentioned that all the AAM composites were prepared with a constant water/solid ratio of 0.4.

2.3. Testing

2.3.1. Microstructure analyses

The microstructure and surface morphology of the surface functionalised wheat straw samples was analysed and compared to the unfunctionalised specimens using scanning electron microscopy (SEM, VEGA3 TESCAN). For each composition, ten straw particle of size 5 mm^3 were analysed to capture reliable statements about the surface changes induced as a result of surface functionalisations. The microstructure of interface between AAM matrix and functionalised straw particles was investigated employing SEM. For each composition, at least ten samples (10 mm^3) were extracted from broken portions of specimens in mechanical test and chromium-coated using a sputter coater to assure the adequate electrical conductivity of AAM samples.

2.3.2. Raman spectroscopy

Raman spectroscopy test was performed in the range of 800–1800 cm^{-1} at room temperature employing inVia Raman Microscope (Renishaw), providing a 785 nm wavelength laser beam.

2.3.3. Thermogravimetric analysis

Thermogravimetric analysis (TGA) and differential thermal analysis (DTA) were conducted to evaluate the impact of surface functionalisations on thermal degradation of straw particles. TGA analysis was performed on 3−4 mg of straw samples under airflow with a heating rate of 10 °C/min using a TA Instrument SDT Q600.

2.3.4. X-ray diffraction

The X-ray diffraction patterns were carried out to investigate the mineralogical composition of the samples after surface functionalisation processes using an Aeris Diffractometer (Bruker) Cu-Kα radiation, 2θ of 5−90°, a wavelength of 1.542 Å, at 40 kV and 40 mA.

2.3.5. Chemical distribution of functional groups

The Fourier transform infrared spectroscopy-Attenuated total reflectance (FTIR-ATR) test (PerkinElmer Spectrum one Spectrometer, UK) was performed to evaluate the chemical functional group distribution of untreated and pre-treated shredded straw samples. Samples were placed on an ATR instrument with a 3x bounce diamond crystal at a 45° incident angle. The instrument produced 20 scans at wavenumbers ranging from 4000 cm^{-1} to 600 cm^{-1} with a 4 cm^{-1} resolution. The average result of a batch of three samples was provided for each composition.

2.3.6. Mechanical property test

After mix preparation, a batch of three prismatic samples (with sizes of 160 × 40 × 40 mm^3) for each composition was casted. All the samples were first heat-cured at 60 °C for 24 h (Mo et al., 2014). The samples were then air-cured at a controlled room temperature (air-curing at 23 ± 2 °C) up to 7 and 90 d. The flexural and compressive strength tests were performed according to BS EN 196–1:2016 by means of Instron 5960 Series Universal Testing System.

2.3.7. Volume of permeable voids percentage

According to ASTM C 642, the boil-water saturation (BWS) technique has been employed to assess the volume of permeable voids percentage (VPV) immediately after sample's curing for 7 d. For each composition, a batch of three prismatic samples of 160 × 40 × 40 mm^3 was casted. The testing method consists of three consecutive steps: (i) samples were placed in the oven for 48 h at 110 °C and weighted (determining the oven-dry mass); (ii) then they were immersed in tap water for 48 h at room temperature and weighted (determining the saturated mass after immersion); (iii) sample's saturated mass after boiling was measured by submerging the samples in boiling water for 5 h. The VPV percentage of each sample was calculated using Eq. (1).

$$VPV \quad (\%) = \left[\frac{(C-A)}{(C-D)}\right] \times 100 \tag{1}$$

Where: VPV is volume of permeable voids (%), A is oven-dry mass (g), C is saturated mass after boiling (g), D is apparent mass of sample in water after immersion (g).

2.3.8. Thermal conductivity measurement

Following ISO 22007–2, thermal property tests were performed using a Hot Disk TPS 2200 device equipped with a 6.4 mm Kapton-insulated sensor. Several thermal parameters, including the thermal conductivity and specific heat of AAM samples modified with different

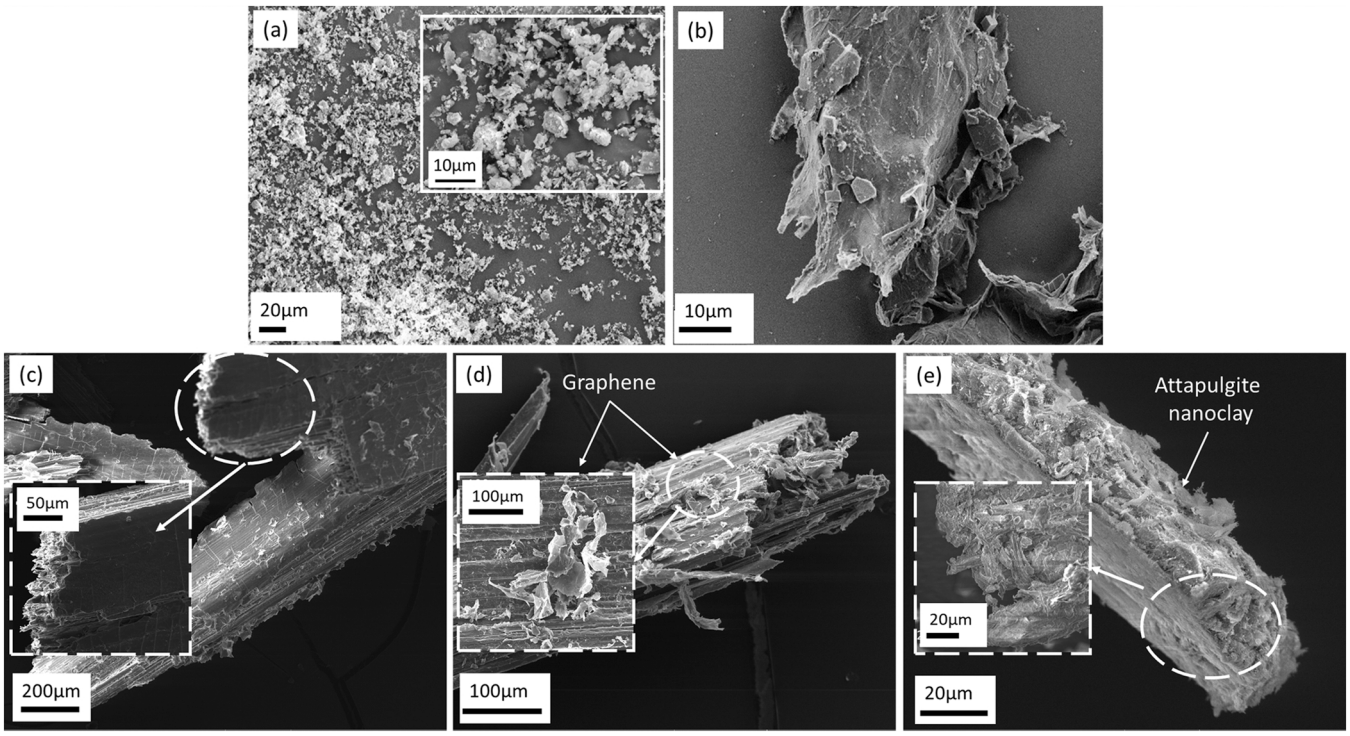

Fig. 3. (a) attapulgite nanoclay, (b) graphene nanoplatelets, and surface profile of (c) H + S pre-treated straw, (d) H + S-G straw, (e) H + S-AT straw.

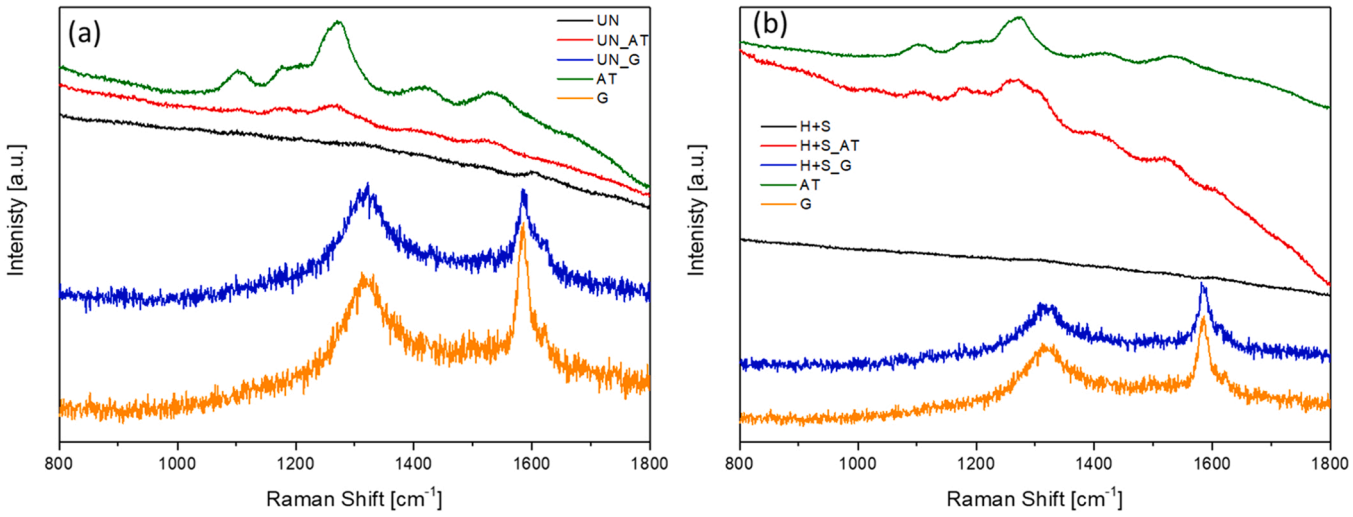

Fig. 4. Raman spectra of a) untreated, and b) pre-treated straw particles and their composites with AT nanoclay and graphene nanoplatelets.

types of wheat straw particles, were evaluated. For each composition, the test was performed on a batch of four 40 × 40 × 40 mm^3 samples after 28 d of curing. In total 12 measurements on 4 cubic specimens were performed with average taken as a value.

3. Results and discussion

3.1. Microstructure of functionalised wheat straw

In Fig. 2(a and b), SEM of attapulgite nanoclay (AT) and graphene nanoplatelets (G) are shown. AT particles employed in this study show a rough surface and angular shape with sharp edges. Isolated graphene nanoplatelets have fringed form and surface wrinkling. However, G particles tend to fluctuate into massive agglomerates, with the unique shape of samples obtained from expanded graphite flakes. The smooth and continuous surface microstructure was observed in H+S sample (see Fig. 3c). The microstructure analyses of straw particles indicate that the surface functionalisations changed the surface appearance of straw particles. The SEM images clearly show an adequate impregnation of straw particles with AT and G particles. Fig. 3e shows characteristic attapulgite nanoclay particles covering the straw, while Fig. 3d shows separated graphene nanoplates attached on the surface of straw.

3.2. Raman investigations

The results of the Raman spectroscopy (see Fig. 4) revealed that G's typical characteristic peaks, i.e. D band 1335 cm^{-1}, due to the carbon lattice disorder typical of edges and defects in the aromatic structure,

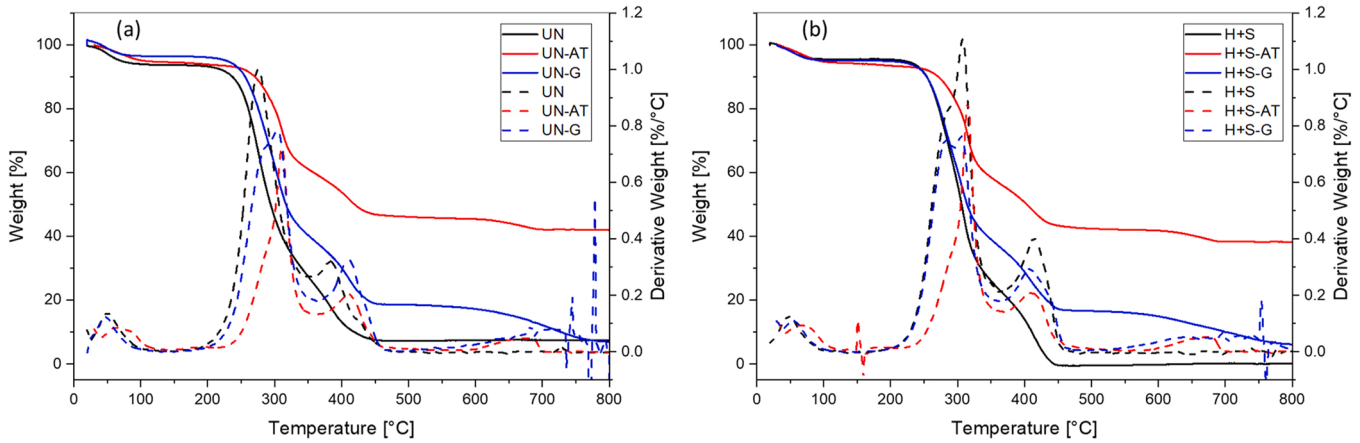

Fig. 5. TGA and DTA thermograms of wheat straw, (a) untreated with and without surface functionalisations, (b) H+S pre-treated with and without surface functionalisations.

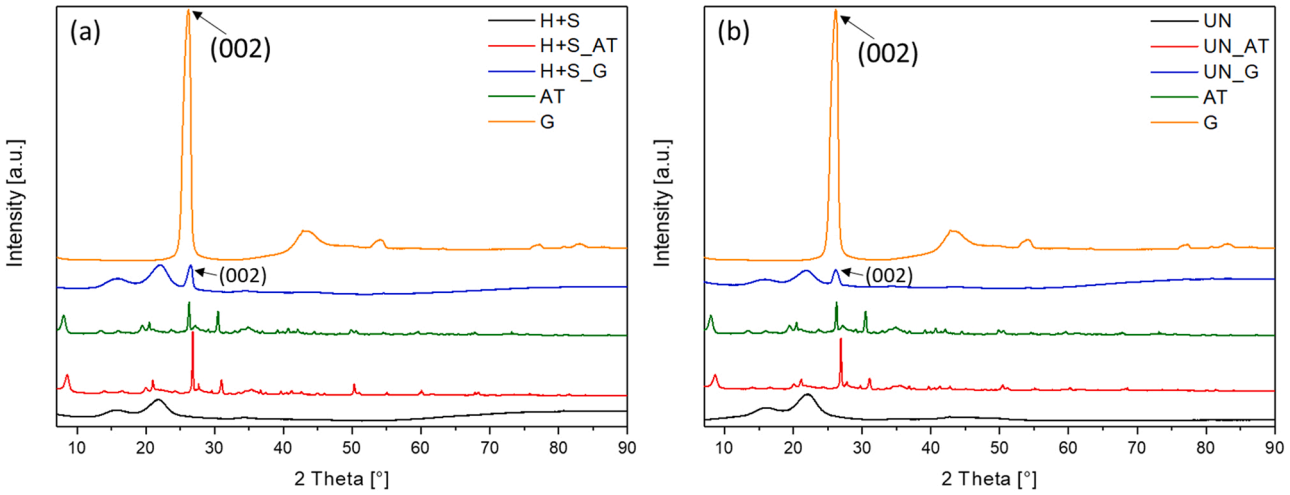

Fig. 6. X-ray diffraction patterns of wheat straw internode with and without pre-treatment and surface functionalisations.

and G band 1585 cm^{-1}, related to the C sp^2 in-plane vibration of the graphene lattice are clearly detected on the surface of straw particles (Owens, 2015). The same peaks are observed in the UN-G and H+S-G composites. In the case of attapulgite nanoclay, a similar signal was observed. The characteristic peaks of AT are visible in the case of UN-AT and H+S-AT samples. None of the above-mentioned peaks are detected on untreated and pre-treated straws (marked in black in both graphs), confirming the effective coverage of AT and G particles in composites.

3.3. Thermogravimetric analysis

Thermogravimetric analysis (Fig. 5) was performed to evaluate the thermal stability of straw samples after surface functionalisations. DTG analyses of the thermograms (Fig. 5-Dash lines) clearly show three distinct stages of thermal degradation. The straw samples first lose weight due to moisture evaporation at 100–150 °C. This is followed by degradation of the cellulose and hemicellulose in the straw sample resulting in severe weight loss in the range of 250–350 °C. The final weight loss occurs as a result of the decomposition of non-cellulosic components - especially in the case of graphene nanoplatelets in the temperature range of 500 – 700 °C. AT nanoclay particles do not decompose in this temperature range (Ergudenler and Ghaly, 1992).

3.4. X-ray diffraction

XRD patterns of AT, G, and functionalised straw samples are shown in Fig. 6 a and b to analyse the crystalline phases of straw specimens. The results indicate that both straw samples functionalised with graphene particles (i.e. H+S-G and UN-G) show different XRD patterns comparing H+S and UN straw samples. After the functionalisation process, the basal reflection peak (002) of graphene flakes around $2\theta = 26.2°$ is clearly observed on the surface of straw particles (Lu, 2017; Lv et al., 2013). In the case of samples functionalised with attapulgite, several crystallographic planes of attapulgite particles, i.e. (110), (200), (040), (231) and (161), at $2\theta = 8.05°$, 13.29°, 19.5°, 26.7°, and 31.02° diffraction peaks were observed in both H+S-AT and UN-AT samples (Tong et al., 2021). The aforementioned results suggest the successful functionalisation process of straw samples modified with graphene and attapulgite.

3.5. Chemical distribution of functional groups analysis

The chemical distribution of pre-treated and untreated straw was characterised using FTIR-ATR spectroscopy (Fig. 7). The aromatic ring stretch of lignin was observed at bands 1595 cm^{-1} and 1510 cm^{-1}, which was slightly attenuated in pre-treated straw samples compared to untreated straw samples (see Fig. 7 i). This suggests that the H+S pre-treatment leads to the partial extraction of lignin. Band 1735 cm^{-1}

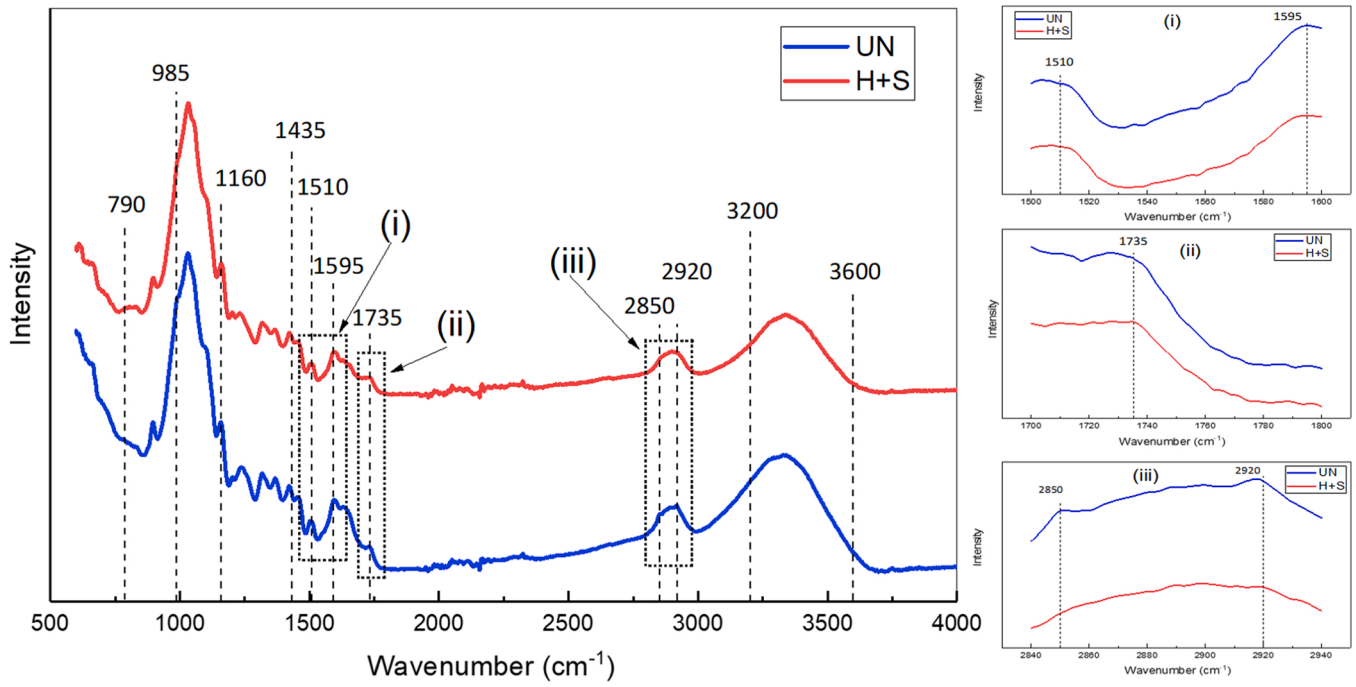

Fig. 7. FTIR-ATR spectrum of untreated (UN) and pre-treated (H+S) straw particles.

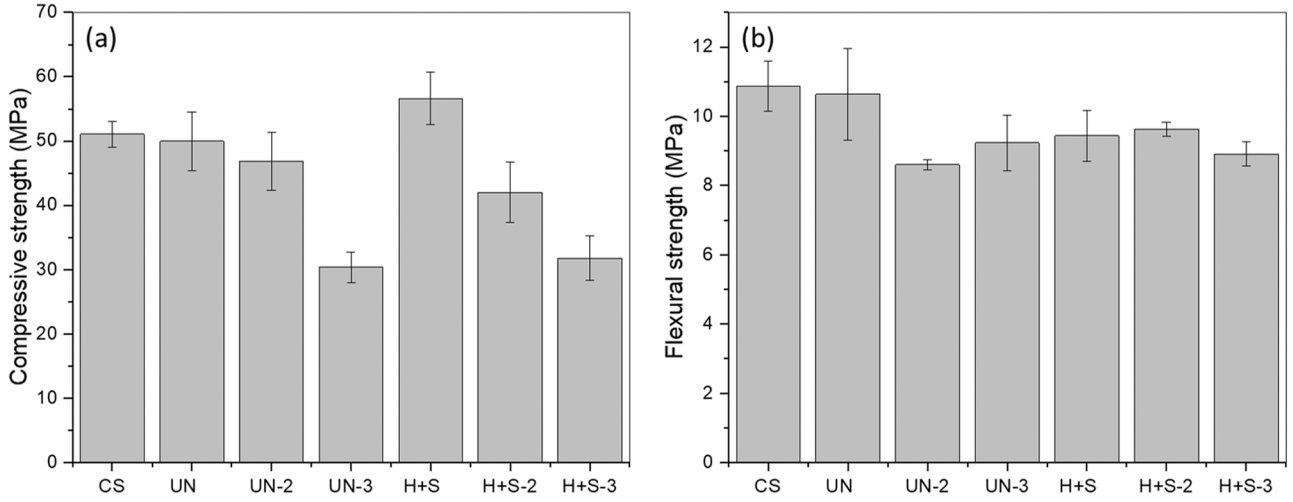

Fig. 8. AAM composites reinforced with different ratios of pre-treated and untreated straw particles (a) compressive strength and (b) flexural strength.

indicates the main components of extractives and hemicellulose, including carboxyl groups in the acids and esters of acetic, *p*-coumeric, ferulic, and uronic acids. As shown in Fig. 7 ii, in comparison to untreated straw, the intensity of this band was diminished in H + S pre-treated sample. The reduction in peak intensity of 1735 cm^{-1} in pre-treated wheat straw implies reduced hemicellulose fractions attributable to the H+S pre-treatment approach. Asymmetric and symmetric CH_2 stretching bands that correspond to the aliphatic fractions of waxes are represented by peaks at bands 2920 cm^{-1} and 2850 cm^{-1}. The results demonstrate that pre-treated straw samples contain a reduced amount of wax and inorganic compounds compared to untreated straw samples (see Fig. 7 iii). This indicates that pre-treatment has a positive effect on the minimisation of inorganic compounds and waxes.

3.6. Mechanical properties analysis

Fig. 8 depicts the mechanical performance of the AAM mix formulations reinforced with 1, 2, and 3 wt.-% of pre-treated and untreated straw after 7 d of curing. As it can be seen in Fig. 8-a, for AAM samples reinforced with both pre-treated and untreated, increasing the dosage of straw particles progressively diminishes the compressive strength. The flexural strength of AAM samples reinforced by untreated straw (Fig. 8-b) first decreased from 10.6 MPa for UN to 8.6 MPa for UN-2. Thereupon, flexural strength of UN-3 was marginally increased, reaching 9.2 MPa, which is still lower than the value registered for the UN sample. The flexural strength results for AAM samples reinforced by pre-treated straw indicated a minor improvement for H+S-2 (i.e. 9.6 MPa) as compared to the H+S (i.e. 9.4 MPa). The incorporation of 3 wt.-% straw (i.e. H+S-3) decreases the flexural strength by 5% comparing the H+S sample. Moreover, with the incorporation of wheat straw particles, the AAM specimens tend to become more ductile, and there was no sharp and sudden rapture upon failure, as opposed to the control specimens, i.e., without straw particles. Similar results were observed in the author's previous works in which the addition of

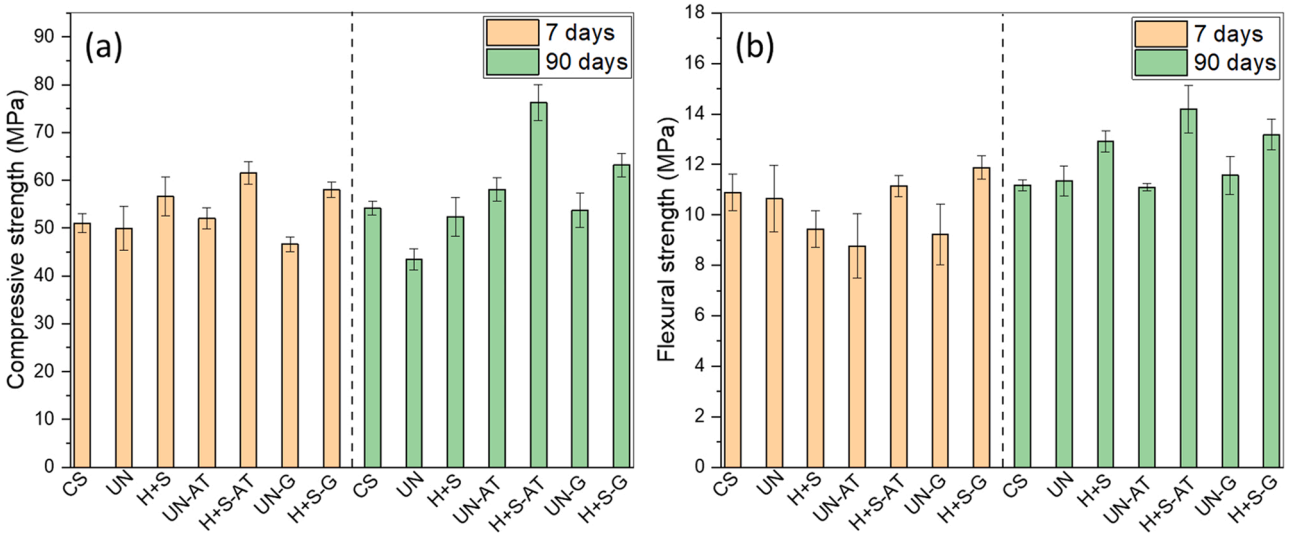

Fig. 9. (a) Flexural, and (b) compressive strength of AAM composites reinforced with different straw particles.

reinforcing biomass materials (i.e., flax and jute fibres) in the cementitious matrix resulted in a ductile behaviour, whereas plain cementitious samples appeared very brittle and shattered into pieces (Ghaffar et al., 2020; Zhou et al., 2013).

As per acquired test results, AAM samples modified with 1 wt.-% of pre-treated and untreated straw (i.e., UN and H+S) displayed superior performance in both flexural and compressive strength. Therefore, the aforementioned compositions were nominated to be used as a suitable mix for the incorporation of functionalising agents to assess if their physical and mechanical properties can be further improved.

Fig. 9 presents the mechanical performance of AAMs reinforced with 1 wt.-% straw particles after 7 and 90 d of curing. All samples showed an increase in flexural strength as the curing duration increased. In general, the flexural strength of the AAM composites is remarkably dependent on the wheat straw strength and the interfacial bond quality (Ghaffar et al., 2017a; Pereira et al., 2013). At 90 d, the addition of pre-treated straw particles (H+S) increases flexural strength by 18% compared to control sample (i.e. from 11 MPa for CS to 13 MPa for H+S). However, the flexural strength of samples reinforced with untreated (UN) straw is statistically comparable to that of the control sample. The impact of straw pre-treatment is clearly beneficial at late ages as there is a 14% increase in flexural strength from the (UN) sample to the pre-treated (H+S) sample after 90 d of curing. This enhancement in the flexural strength due to the pre-treatment could confirm the reduction of amorphous hemicellulose, lignin, and waxes content present in wheat straw (see section 3.1.5) that can promote the activation kinetics of cement-free binders (Ye et al., 2018; Zhou et al., 2020).

The higher tensile strength of H+S straw particles can also affect the AAMs' mechanical performance compared to untreated counterparts. Ghaffar et al. (2017a) reported that the tensile strength of individual wheat straw internode achieved tensile strengths of 89 MPa after H+S pre-treatment, that is 35% higher than that of untreated samples (Ghaffar et al., 2017a). Surface functionalisations were proposed to act as a crosslink improving the interfacial bonding between straw and matrices (Scaffaro et al., 2020; Zhu et al., 2019). Both surface functionalising materials (i.e. graphene and attapulgite) have proven to be effective in increasing the mechanical performance of AAMs' reinforced with pre-treated straw samples. The impact of pre-treatment on surface functionalisation is clear with attapulgite surface functionalised samples, i.e., H+S-AT, in which the flexural strength increased by 27% at 7 d and 28% at 90 d compared to UN-AT samples. As shown in Fig. 9-b, H+S-AT also attains a higher compressive strength at 7 d (from 52 MPa to 62 MPa) and at 90 d (from 58 MPa to 76 MPa) compared to UN-AT samples. The high strength gains of H+S-AT can be justified, as demonstrated in Fig. 10, where attapulgite particles on the surface of pre-treated straw (i.e. H+S-AT) effectively fill in the gaps between the functionalised straw particles and matrix, creating intimate interfacial bonding. The delamination is remarkably reduced as a result of AT surface functionalisation.

Besides the positive effect of surface functionalisations on the straw-matrix interfacial bonding, attapulgite covering layer can act as a physical barrier protecting the wheat straw particles from exposure to high-alkaline environment hence preventing the decay in structural integrity during aging of AAM. In general, the high alkaline environment of AAM composites can severely influence the amorphous constituents of biomass materials. As reported by Wei et al. (2015), partial or complete alkaline degradation of biomass main components (i.e. cellulose, hemicellulose, and lignin) in cementitious composites leads to reduced structural integrity of the lignocellulosic particles cell wall hence weakens the interface bonding quality with the matrix (Wei and Meyer, 2015). This can results in a reduction of mechanical performance of composites reinforced with natural fibres/particles (Wei and Meyer, 2016). This effect was observed (see Fig. 9-b) in compressive strength reduction of not functionalised samples (i.e. UN and H+S) from 7 d to 90 d. For UN and H+S, a 15% and 8% drop in compressive strength was registered, respectively. In contrast, the compressive strength of all the AAM samples reinforced with surface functionalised straw particles increased with curing time. The maximum enhancement in both flexural and compressive strength at 90 d was recorded for H+S-AT in which flexural strength improved by 29% compared to 7 d samples. Compressive strength of H+S-AT composite also increased from 61 MPa at 7 d to 76 MPa at 90 d.

3.7. Volume of permeable voids evaluation

Fig. 11 shows the volume of permeable voids (VPV) in AAM samples reinforced with straw particles. In general, the VPV does not represent the total porosity; however, it identifies the volume of capillary pores in porous materials, which can be utilised as a parameter to approximately predict the cementitious material's overall water penetration (Lau et al., 2018; Mannan et al., 2016). The results revealed that the incorporation of straw in AAM reduces the VPV percentage of the composites compared to the control sample. In addition, it can be seen that the incorporation of pre-treated straw was found to be more effective in water penetration reduction. The reason is attributed to the stronger straw-matrix bonding, which inhibits the transfer of water molecules

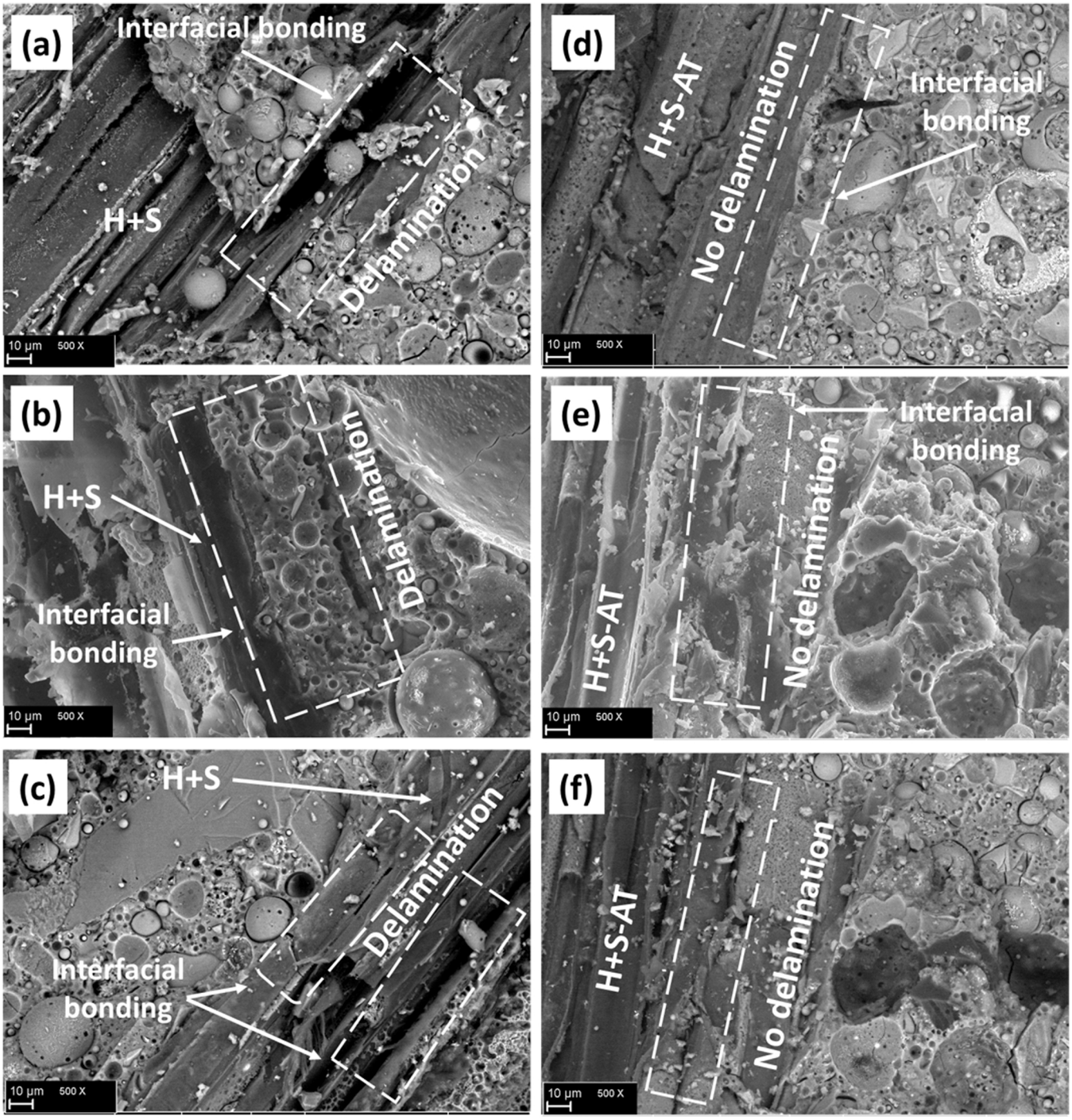

Fig. 10. SEM micrographs of (a, b, and c) H+S samples, (d, e, and f) H+S-AT samples.

into the samples (Huang et al., 2021). The results indicated that the permeability of H+S-AT and H+S-G are 12% and 7% lower than UN-AT and UN-G samples, respectively. Similar to the mechanical performance results, this could be related to the better compatibility of pre-treated straw particles with surface functionalisations which leads to a denser structure within the cement-free composites, therefore, reduces the water intake.

3.8. Thermal conductivity

Fig. 12 presents the results of specific heat and thermal conductivity of AAM specimens determined with hot disk method. All tested specimens exhibited comparable values of specific heat. Similarly, no substantial differences in the thermal conductivity (TC) values of AAM samples were observed. Despite marginal differences between the specimens, general conclusions can be drawn. It is known that thermal conductivity of composites is linked to the TC of its constituents with major contributions from the material's density (Strzałkowski et al., 2021). All AAM specimens were varied only in terms of type of straw used which was occupying 1 wt.-% of AAM material. Control samples (CS) exhibited thermal conductivity of 1.279 W/mK, while incorporation of untreated straw particles (UN) resulted in insignificant reduction of TC, i.e., 1.210 W/mK. This could be attributed to low density of wheat straw particles along with lower TC of straw than other AAM

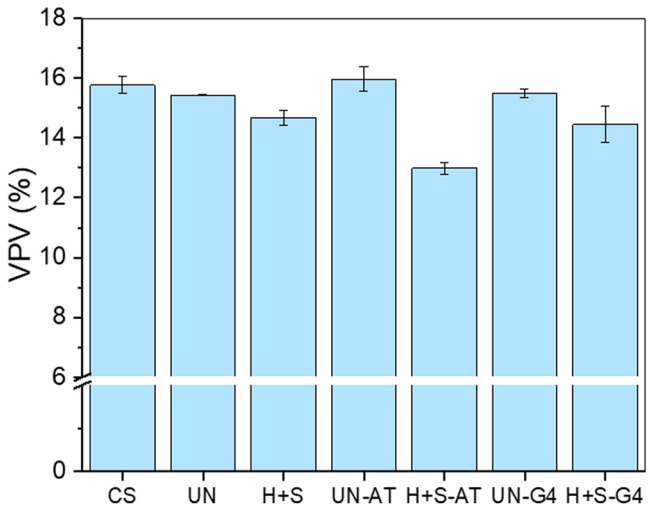

Fig. 11. Volume of permeable voids (VPV) of AAM composites modified with different straw particles.

constituents (Insulating et al., 2021). Slight increase of thermal conductivity, when compared to CS, was observed in specimens with pre-treated straw (H+S). This might be due to the partial removal of wax and silicate from straw as a result of boiling and steaming process. In general, increasing the gaps between matrix and straw particles that serve as phonon scattering centres take up a fraction of the heat conduction volume of the material, resulting in a decrease in composite thermal conductivity. Removing hydrophobic components, however, results in a more compact structure, lowering the gap or delamination between matrix and straw particles, thus improving thermal conductivity. Functionalisation of the straw surface with attapulgite (H+S-AT) resulted in slight reduction of TC, when compared to H+S. In case of untreated straw specimen (UN-AT) no alteration in TC was observed. It is worth noting that attapulgite has low thermal conductivity according to the literature (Liu et al., 2016). In contrary, functionalising straw surface with graphene (H+S-G) resulted in the highest TC among all specimens which was 13% higher than CS. UN-G sample, also showed a slightly higher TC values, however, the increment was lower than that of H+S-G.

As reported by Zhang et al. (2020) even a small dosage of graphene (0.05 wt.-%) results in increased TC of cementitious composites. Similarly, Chu et al. (2017) reported a 22% increase of thermal conductivity when 0.1 wt.-% of graphene was introduced into concrete. The thermal conductivity of AAM have been studied by several authors, where they reported a range of TC values, e.g., between 0.65 W/mK and 0.8 W/mK (Duxson et al., 2006; Subaer, 2007), which is higher than the 0.53 W/mK recorded for traditional OPC-based cementitious composites (Demirboğa, 2003). The results are consistent with the density-dependency hypothesis, as the inclusion of aggregate increases the bulk density of the sample. Quartz's high thermal conductivity (approximately 5.9–11.1 W/mK) contributes to a significant increase in the TC of AAM composites (Van Riessen et al., 2009).

4. Conclusions

An alkali-activated material reinforced with wheat straw particles was developed, employing pre-treated and surface functionalised straw particles as reinforcing agents. Characterisation tests indicated substantial changes to wheat straw particles after pre-treatment and surface functionalisations, all of which induced a remarkable impact on the performance of wheat straw particles. However, Surface functionalisations did not contribute to substantial enhancements of AAM's thermal properties and differences are rather marginal.

Using attapulgite nanoclay as a surface functionalising agent on the pre-treated straw particles was found to be the best performing sample in terms of mechanical performance improvements and volume of permeable voids reduction. The effect is most likely associated with enhancements on interfacial bonding between the straw and the AAM matrix due to the presence of attapulgite crosslink agent.

The alkali-activated cement-free composites reinforced with pre-treated and surface functionalised wheat straw particles developed in this study demonstrate a promising breakthrough that can be used as a benchmark in the fabrication of low-carbon AAM composites. However, future research could concentrate on solving the issues with inclusion of higher percentages of straw reinforcements.

CRediT authorship contribution statement

Mehdi Chougan: Data curation, Methodology, Writing – review & editing. **Seyed Hamidreza Ghaffar:** Conceptualization, Methodology, Supervision, Writing – review & editing. **Pawel Sikora:** Writing – original draft, Data curation. **Ewa Mijowska:** Writing – original draft, Data curation. **Wojciech Kukułka:** Writing – original draft, Data curation. **Dietmar Stephan:** Writing – review & editing.

Declaration of Competing Interest

The authors declare that they have no known competing financial

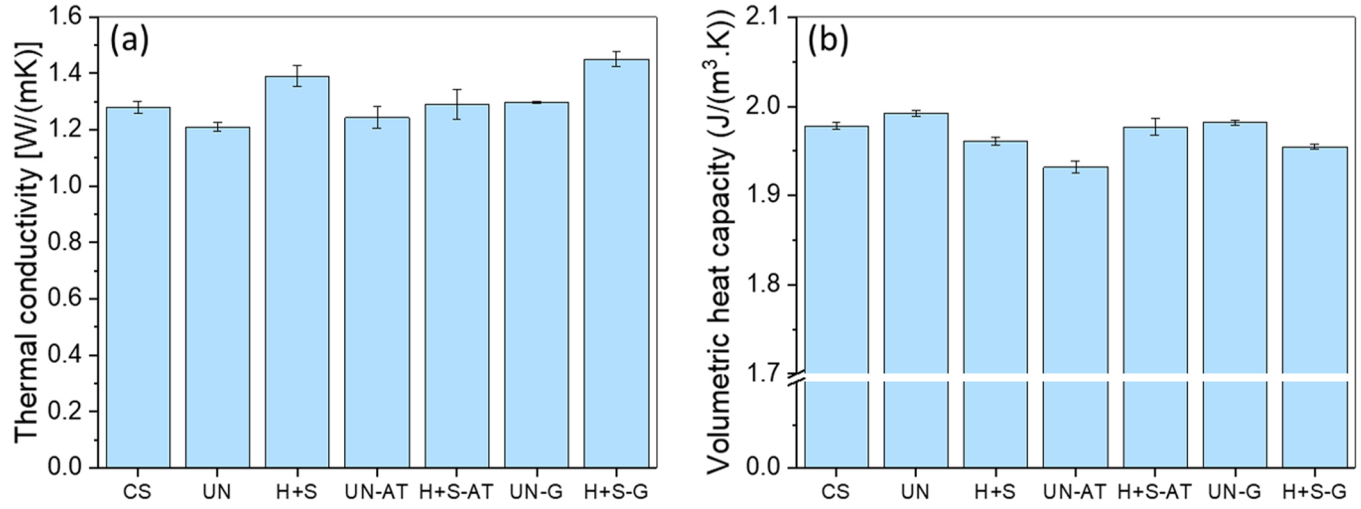

Fig. 12. (a) Thermal conductivity and (b) heat capacity of AAMs modified with different straw particles.

interests or personal relationships that could have appeared to influence the work reported in this paper.

Acknowledgements

This work was funded as part of the HP-CSB project, which has received funding from the Engineering and Physical Sciences Research Council with the following reference: EP/S026487/1.

The authors acknowledge Nanesa S.r.l for graphene material supply and Dr. C. Lehmann from TU Berlin for SEM assessments.

References

Abirami, R., Vijayan, D., John, S.J., Albert, A., Alex, A.K., 2020. Exp. Study Concr. Prop. Using Pineapple Leaf Fiber, 11, pp. 913–920 doi: 10.34218/IJARET.11.6.2020.082.

Albar, A., Chougan, M., Al- Kheetan, M.J., Swash, M.R., Ghaffar, S.H., 2020. Effective extrusion-based 3D printing system design for cementitious-based materials. Results Eng. 6, 100135 https://doi.org/10.1016/j.rineng.2020.100135.

Alengaram, U.J., Muhit, B.A., Jumaat, Al, Bin, M.Z., 2013. Utilization of oil palm kernel shell as lightweight aggregate in concrete - a review. Constr. Build. Mater. 38, 161–172. https://doi.org/10.1016/j.conbuildmat.2012.08.026.

Chougan, M., Ghaffar, S.H., Al-Kheetan, M.J., Gecevicius, M., 2020a. Wheat straw pre-treatments using eco-friendly strategies for enhancing the tensile properties of bio-based polylactic acid composites. Ind. Crop. Prod. 155. https://doi.org/10.1016/j.indcrop.2020.112836.

Chougan, M., Ghaffar, S.H., Sikora, P., Chung, S.Y., Rucinska, T., Stephan, D., Albar, A., Swash, M.R., 2021. Investigation of additive incorporation on rheological, microstructural and mechanical properties of 3D printable alkali-activated materials. Mater. Des. 202. https://doi.org/10.1016/j.matdes.2021.109574.

Chougan, M., Hamidreza Ghaffar, S., Jahanzat, M., Albar, A., Mujaddedi, N., Swash, R., 2020b. The influence of nano-additives in strengthening mechanical performance of 3D printed multi-binder geopolymer composites. Constr. Build. Mater. 250, 118928 https://doi.org/10.1016/j.conbuildmat.2020.118928.

Chu, H., Yan, Jiang, Yang, J., Sun, W., Zhang, M., 2017. Mechanical and thermal properties of graphene sulfonate nanosheet reinforced sacrificial concrete at elevated temperatures. Constr. Build. Mater. 153, 682–694. https://doi.org/10.1016/j.conbuildmat.2017.07.157.

da Silva Alves, L.C., dos Reis Ferreira, R.A., Bellini Machado, L., de Castro Motta, L.A., 2019. Optimization of metakaolin-based geopolymer reinforced with sisal fibers using response surface methology. Ind. Crop. Prod. 139, 111551 https://doi.org/10.1016/j.indcrop.2019.111551.

Demirboğa, R., 2003. Thermo-mechanical properties of sand and high volume mineral admixtures. Energy Build. 35, 435–439. https://doi.org/10.1016/S0378-7788(02)00159-7.

Department for Environment Food & Rural Affairs DEFRA, 2020. Farming Statistics – First estimates of 2020 UK wheat and barley production, National Statitstics.

Duxson, P., Lukey, G.C., Van Deventer, J.S.J., 2006. Thermal conductivity of metakaolin geopolymers used as a first approximation for determining gel interconnectivity. Ind. Eng. Chem. Res. 45, 7781–7788. https://doi.org/10.1021/ie060187o.

Elbashiry, E.M.A., Chen, J., Tuo, W., Ren, Y., Guo, Z., 2018. Review of the pretreatment methods for wheat straw building materials. J. Reinf. Plast. Compos. 37, 35–48. https://doi.org/10.1177/0731684417730442.

Ergudenler, A., Ghaly, A., 1992. Determination of reaction kinetics of wheat straw using thermogravimetric analysis. Appl. Biochem. Biotechnol. 34. https://doi.org/10.1007/BF02920535.

Fan, Q., Han, G., Cheng, W., Tian, H., Wang, D., Xuan, L., 2018. Effect of intercalation structure of organo-modified montmorillonite/polylactic acid on wheat straw fiber/polylactic acid composites. Polymers 1–14. https://doi.org/10.3390/polym10080896.

Ghaffar, S.H., Al-Kheetan, M., Ewens, P., Wang, T., Zhuang, J., 2020. Investigation of the interfacial bonding between flax/wool twine and various cementitious matrices in mortar composites. Constr. Build. Mater. 239, 117833 https://doi.org/10.1016/j.conbuildmat.2019.117833.

Ghaffar, S.H., Fan, M., 2015. Differential behaviour of nodes and internodes of wheat straw with various pre-treatments. Biomass Bioenergy 83, 373–382. https://doi.org/10.1016/j.biombioe.2015.10.020.

Ghaffar, S.H., Fan, M., 2013. Structural analysis for lignin characteristics in biomass straw. Biomass Bioenergy 57, 264–279. https://doi.org/10.1016/j.biombioe.2013.07.015.

Ghaffar, S.H., Fan, M., McVicar, B., 2017a. Interfacial properties with bonding and failure mechanisms of wheat straw node and internode. Compos. Part A Appl. Sci. Manuf. 99, 102–112. https://doi.org/10.1016/j.compositesa.2017.04.005.

Ghaffar, S.H., Fan, M., Zhou, Y., Abo Madyan, O., 2017b. Detailed analysis of wheat straw node and internode for their prospective efficient utilization. J. Agric. Food Chem. 65, 9069–9077. https://doi.org/10.1021/acs.jafc.7b03304.

Ghaffar, S.H., Madyan, O.A., Fan, M., Corker, J., 2018. The influence of additives on the interfacial bonding mechanisms between natural fibre and biopolymer composites. Macromol. Res. 26, 851–863. https://doi.org/10.1007/s13233-018-6119-8.

Glé, P., Massossa-Telo, G., Hellouin de Menibus, A., Degrave-Lemeurs, M., Gourdon, E., 2021. Characterization and modelling of the sound reduction of hemp-clay walls in buildings. J. Build. Eng. 40. https://doi.org/10.1016/j.jobe.2021.102315.

Guan, X.K., Wei, L., Turner, N.C., Ma, S.C., Yang, M., Da, Wang, T.C., 2020. Improved straw management practices promote in situ straw decomposition and nutrient release, and increase crop production. J. Clean. Prod. 250, 119514 https://doi.org/10.1016/j.jclepro.2019.119514.

Habert, G., D'Espinose De Lacaillerie, J.B., Roussel, N., 2011. An environmental evaluation of geopolymer based concrete production: reviewing current research trends. J. Clean. Prod. 19, 1229–1238. https://doi.org/10.1016/j.jclepro.2011.03.012.

Hakamy, A., Shaikh, F.U.A., Low, I.M., 2016. Effect of calcined nanoclay on the durability of NaOH treated hemp fabric-reinforced cement nanocomposites. Mater. Des. 92, 659–666. https://doi.org/10.1016/j.matdes.2015.12.097.

Heede, P.Van Den, Belie, N.De, 2012. Environmental impact and life cycle assessment (LCA) of traditional and ' green ' concretes: literature review and theoretical calculations. Cem. Concr. Compos. 34, 431–442. https://doi.org/10.1016/j.cemconcomp.2012.01.004.

Huang, Y., Tan, J., Xuan, X., Liu, L., Xie, M., Liu, H., Yu, S., Zheng, G., 2021. Study on untreated and alkali treated rice straw reinforced geopolymer composites. Mater. Chem. Phys. 262, 124304 https://doi.org/10.1016/j.matchemphys.2021.124304.

Hýsková, P., Hýsek, Š., Schönfelder, O., Šedivka, P., Lexa, M., Jarský, V., 2020. Utilization of agricultural rests: straw-based composite panels made from enzymatic modified wheat and rapeseed straw. Ind. Crop. Prod. 144. https://doi.org/10.1016/j.indcrop.2019.112067.

Insulating, S.T., Stevulova, N., Estokova, A., 2021. Heat Transfer in Straw-Based Thermal Insulating Materials.

Kathiravan, N.S., Manojkumar, R., Jayakumar, P., Kumaraguru, J., Jayanthi, V., 2021. State of art of review on bamboo reinforced concrete. Mater. Today Proc. 45, 1063–1066. https://doi.org/10.1016/j.matpr.2020.03.159.

Khazma, M., Goullieux, A., Dheilly, R.M., Rougier, A., Quéneudec, M., 2014. Optimization of flax shive-cementitious composites: Impact of different aggregate treatments using linseed oil. Ind. Crop. Prod. 61, 442–452. https://doi.org/10.1016/j.indcrop.2014.07.041.

Lamastra, F.R., Chougan, M., Marotta, E., Ciattini, S., Ghaffar, S.H., Caporali, S., Vivio, F., Montesperelli, G., Ianniruberto, U., Al-Kheetan, M.J., Bianco, A., 2021. Toward a better understanding of multifunctional cement-based materials: the impact of graphite nanoplatelets (GNPs). Ceram. Int. 47, 20019–20031. https://doi.org/10.1016/j.ceramint.2021.04.012.

Lau, P.C., Teo, D.C.L., Mannan, M.A., 2018. Mechanical, durability and microstructure properties of lightweight concrete using aggregate made from lime-treated sewage sludge and palm oil fuel ash. Constr. Build. Mater. 176, 24–34. https://doi.org/10.1016/j.conbuildmat.2018.04.179.

Liu, Y., Wang, X., Wang, Y., Tang, Z., Makarenko, T., Guloy, A., Zhang, Q., Ren, Z., 2016. Ultra-low thermal conductivities of hot-pressed attapulgite and its potential as thermal insulation material. Appl. Phys. Lett. 108. https://doi.org/10.1063/1.4943626.

Lu, L., Ouyang, D., 2017. Properties of cement mortar and ultra-high strength concrete incorporating graphene oxide nanosheets. Nanomaterials 1–14. https://doi.org/10.3390/nano7070187.

Lv, S., Ma, Y., Qiu, C., Zhou, Q., 2013. Regulation of GO on cement hydration crystals and its toughening effect. Mag. Concr. Res. 65, 1246–1254. https://doi.org/10.1680/macr.13.00190.

Mannan, M.A., Ibrahim, M.Z.M., Ibrahim, A., Jainudin, N.A., Yusuh, N.A., 2016. Performance-based durability indicators of different concrete grades made by the local ready mixed company: preliminary results. Procedia - Soc. Behav. Sci. 224, 620–625. https://doi.org/10.1016/j.sbspro.2016.05.452.

McLellan, B.C., Williams, R.P., Lay, J., Van Riessen, A., Corder, G.D., 2011. Costs and carbon emissions for geopolymer pastes in comparison to ordinary portland cement. J. Clean. Prod. 19, 1080–1090. https://doi.org/10.1016/j.jclepro.2011.02.010.

Merabti, S., Kenai, S., Belarbi, R., Khatib, J., 2021. Thermo-mechanical and physical properties of waste granular cork composite with slag cement. Constr. Build. Mater. 272, 121923 https://doi.org/10.1016/j.conbuildmat.2020.121923.

Meshram, R.B., Kumar, S., 2021. Comparative life cycle assessment (LCA) of geopolymer cement manufacturing with Portland cement in Indian context. Int. J. Environ. Sci. Technol. https://doi.org/10.1007/s13762-021-03336-9.

Mishra, S., Mohanty, A.K., Drzal, L.T., Misra, M., Hinrichsen, G., 2004. A review on pineapple leaf fibers, sisal fibers and their biocomposites. Macromol. Mater. Eng. 289, 955–974. https://doi.org/10.1002/mame.200400132.

Mo, B.H., Zhu, H., Cui, X.M., He, Y., Gong, S.Y., 2014. Effect of curing temperature on geopolymerization of metakaolin-based geopolymers. Appl. Clay Sci. 99, 144–148. https://doi.org/10.1016/j.clay.2014.06.024.

Mohamed, M.A.S., Ghorbel, E., Wardeh, G., 2010. Valorization of micro-cellulose fibers in self-compacting concrete. Constr. Build. Mater. 24, 2473–2480. https://doi.org/10.1016/j.conbuildmat.2010.06.009.

Ouellet-Plamondon, C., Habert, G., 2015. Life cycle assessment (LCA) of alkali-activated cements and concretes. Handbook of Alkali-Activated Cements, Mortars and Concretes. Woodhead Publishing Limited. https://doi.org/10.1533/9781782422884.5.663.

Owens, F.J., 2015. Raman and surface-enhanced Raman spectroscopy evidence for oxidation-induced decomposition of graphite. Mol. Phys. 113, 1280–1283. https://doi.org/10.1080/00268976.2014.986237.

Pacheco-Torgal, F., Jalali, S., 2011. Cementitious building materials reinforced with vegetable fibres: a review. Constr. Build. Mater. 25, 575–581. https://doi.org/10.1016/j.conbuildmat.2010.07.024.

Parcesepe, E., De Masi, R.F., Lima, C., Mauro, G.M., Pecce, M.R., Maddaloni, G., 2021. Assessment of mechanical and thermal properties of hemp-lime mortar. Materials 1–24. https://doi.org/10.3390/ma14040882.

Pereira, C.L., Savastano, H., Payá, J., Santos, S.F., Borrachero, M.V., Monzó, J., Soriano, L., 2013. Use of highly reactive rice husk ash in the production of cement matrix reinforced with green coconut fiber. Ind. Crop. Prod. 49, 88–96. https://doi.org/10.1016/j.indcrop.2013.04.038.

Satyanarayana, K.G., Arizaga, G.G.C., Wypych, F., 2009. Biodegradable composites based on lignocellulosic fibers-an overview. Prog. Polym. Sci. 34, 982–1021. https://doi.org/10.1016/j.progpolymsci.2008.12.002.

Scaffaro, R., Maio, A., Gulino, E.F., Pitarresi, G., 2020. Lignocellulosic fillers and graphene nanoplatelets as hybrid reinforcement for polylactic acid: effect on mechanical properties and degradability. Compos. Sci. Technol. 190, 108008 https://doi.org/10.1016/j.compscitech.2020.108008.

Sikora, P., Chougan, M., Cuevas, K., Liebscher, M., Mechtcherine, V., Ghaffar, S.H., Liard, M., Lootens, D., Krivenko, P., Sanytsky, M., Stephan, D., 2021. The effects of nano- and micro-sized additives on 3D printable cementitious and alkali-activated composites: a review. Appl. Nanosci. https://doi.org/10.1007/s13204-021-01738-2.

Strzałkowski, J., Sikora, P., Chung, S.Y., Abd Elrahman, M., 2021. Thermal performance of building envelopes with structural layers of the same density: lightweight aggregate concrete versus foamed concrete. Build. Environ. 196. https://doi.org/10.1016/j.buildenv.2021.107799.

Subaer, Van Riessen, A., 2007. Thermo-mechanical and microstructural characterisation of sodium-poly(sialate-siloxo) (Na-PSS) geopolymers. J. Mater. Sci. 42, 3117–3123. https://doi.org/10.1007/s10853-006-0522-9.

Tian, S.Q., Zhao, R.Y., Chen, Z.C., 2018. Review of the pretreatment and bioconversion of lignocellulosic biomass from wheat straw materials. Renew. Sustain. Energy Rev. 91, 483–489. https://doi.org/10.1016/j.rser.2018.03.113.

Tong, H., Liu, X., Liu, Y., Zhang, H., Li, X., 2021. Polyaniline modified attapulgite incorporated in alkyd paint for carbon steel corrosion inhibition. Corros. Eng. Sci. Technol. 0, 1–8. https://doi.org/10.1080/1478422x.2021.1931646.

Tran Le, A.D., Maalouf, C., Mai, T.H., Wurtz, E., Collet, F., 2010. Transient hygrothermal behaviour of a hemp concrete building envelope. Energy Build. 42, 1797–1806. https://doi.org/10.1016/j.enbuild.2010.05.016.

Van Riessen, A., Rickard, W., Sanjayan, J., 2009. Thermal properties of geopolymers. Geopolymers 315–342. https://doi.org/10.1533/9781845696382.2.315.

Vo, L.T.T., Navard, P., 2016. Treatments of plant biomass for cementitious building materials – a review. Constr. Build. Mater. 121, 161–176. https://doi.org/10.1016/j.conbuildmat.2016.05.125.

Walbrück, K., Drewler, L., Witzleben, S., Stephan, D., 2021. Factors influencing thermal conductivity and compressive strength of natural fiber-reinforced geopolymer foams. Open Ceram. 5, 100065 https://doi.org/10.1016/j.oceram.2021.100065.

Walbrück, K., Maeting, F., Witzleben, S., Stephan, D., 2020. Natural fiber-stabilized geopolymer foams-A review. Materials 13. https://doi.org/10.3390/ma13143198.

Wambua, P., Ivens, J., Verpoest, I., 2003. Natural fibres: can they replace glass in fibre reinforced plastics? Compos. Sci. Technol. 63, 1259–1264. https://doi.org/10.1016/S0266-3538(03)00096-4.

Wei, J., Meyer, C., 2016. Utilization of rice husk ash in green natural fiber-reinforced cement composites: mitigating degradation of sisal fiber. Cem. Concr. Res. 81, 94–111. https://doi.org/10.1016/j.cemconres.2015.12.001.

Wei, J., Meyer, C., 2015. Degradation mechanisms of natural fiber in the matrix of cement composites. Cem. Concr. Res. 73, 1–16. https://doi.org/10.1016/j.cemconres.2015.02.019.

Ye, H., Zhang, Y., Yu, Z., Mu, J., 2018. Effects of cellulose, hemicellulose, and lignin on the morphology and mechanical properties of metakaolin-based geopolymer. Constr. Build. Mater. 173, 10–16. https://doi.org/10.1016/j.conbuildmat.2018.04.028.

Zhang, N., She, W., Du, F., Xu, K., 2020. Experimental study on mechanical and functional properties of reduced graphene oxide/cement composites. Materials 13. https://doi.org/10.3390/ma13133015.

Zhou, B., Wang, L., Ma, G., Zhao, Xin, Zhao, Xianhui, 2020. Preparation and properties of bio-geopolymer composites with waste cotton stalk materials. J. Clean. Prod. 245, 118842 https://doi.org/10.1016/j.jclepro.2019.118842.

Zhou, X., Ghaffar, S.H., Dong, W., Oladiran, O., Fan, M., 2013. Fracture and impact properties of short discrete jute fibre-reinforced cementitious composites. Mater. Des. 49, 35–47. https://doi.org/10.1016/j.matdes.2013.01.029.

Zhu, L., Qiu, J., Liu, W., Sakai, E., 2019. Mechanical and thermal properties of rice Straw / PLA modi fi ed by nano Attapulgite / PLA interfacial layer. Compos. Commun. 18–21. https://doi.org/10.1016/j.coco.2019.02.001.